Supplementary Information

Breathable and Skin-Conformal Electronic Skin with Dual-modality Synchronous Perception of Pressure and Temperature

Hao Zhu[1,2‡], Zhelin Jin[1‡], Tie Li[2,3*], Guanggui Cheng[1*], Jianning Ding[1,4]

[1] Institute of Intelligent Flexible Mechatronics, Jiangsu University, Zhenjiang 212013, PR China
[2] i-Lab Suzhou Institute of Nano-Tech and Nano-Bionics (SINANO), Chinese Academy of Sciences (CAS), Suzhou 215123, P. R. China
[3] Jiangxi Institute of Nanotechnology, Nanchang 330200, China
[4] School of Mechanical Engineering, Yangzhou University, Yangzhou 225009, PR China

[*]Corresponding authors Email: tli2014@sinano.ac.cn, ggcheng@ujs.edu.cn.

[‡] These authors contributed equally to this work and should be considered co-first authors.

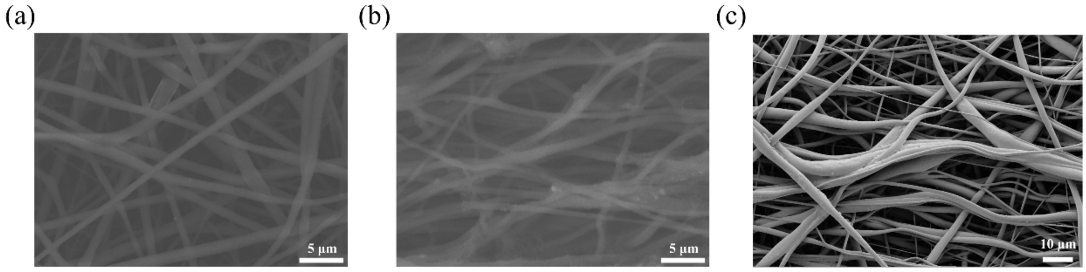

Fig. S1. (a) SEM image of the nanofiber membrane fabricated by the process parameters in this paper. (b) SEM image of the nanofiber membrane fabricated at a high solution concentration of 40 wt% with other process parameters remaining unchanged. (c) SEM image of the nanofiber membrane fabricated at a high relative humidity of 50±3% with other process parameters remaining unchanged.

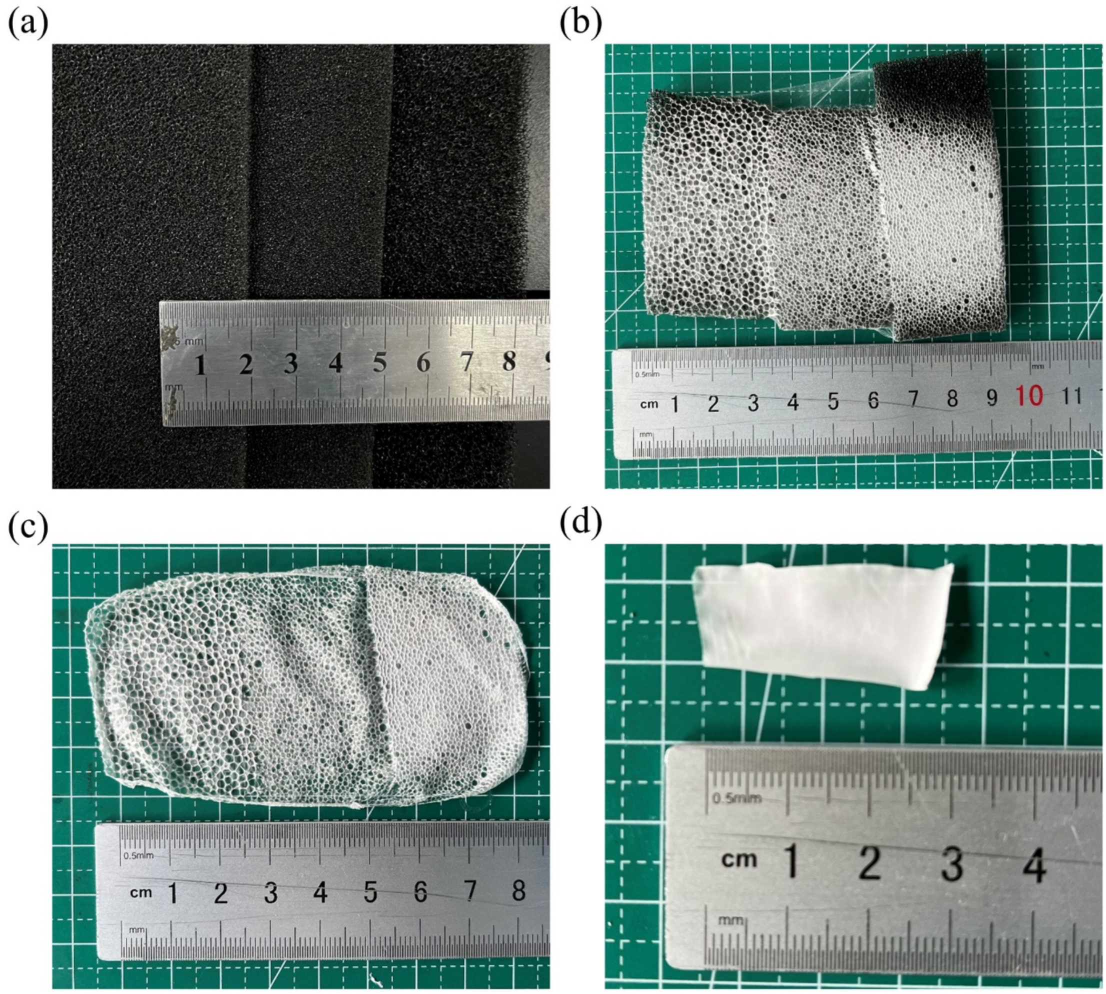

Fig. S2. (a) The optical photograph of foams with three mesh sizes (From left to right: 60 mesh, 40 mesh, 20 mesh); (b) The optical photograph of fibrous membranes on foams of different mesh sizes; (c) The optical photograph of ordered porous fibrous membranes with different pore sizes; (d) The optical photograph of random porous fibrous membrane.

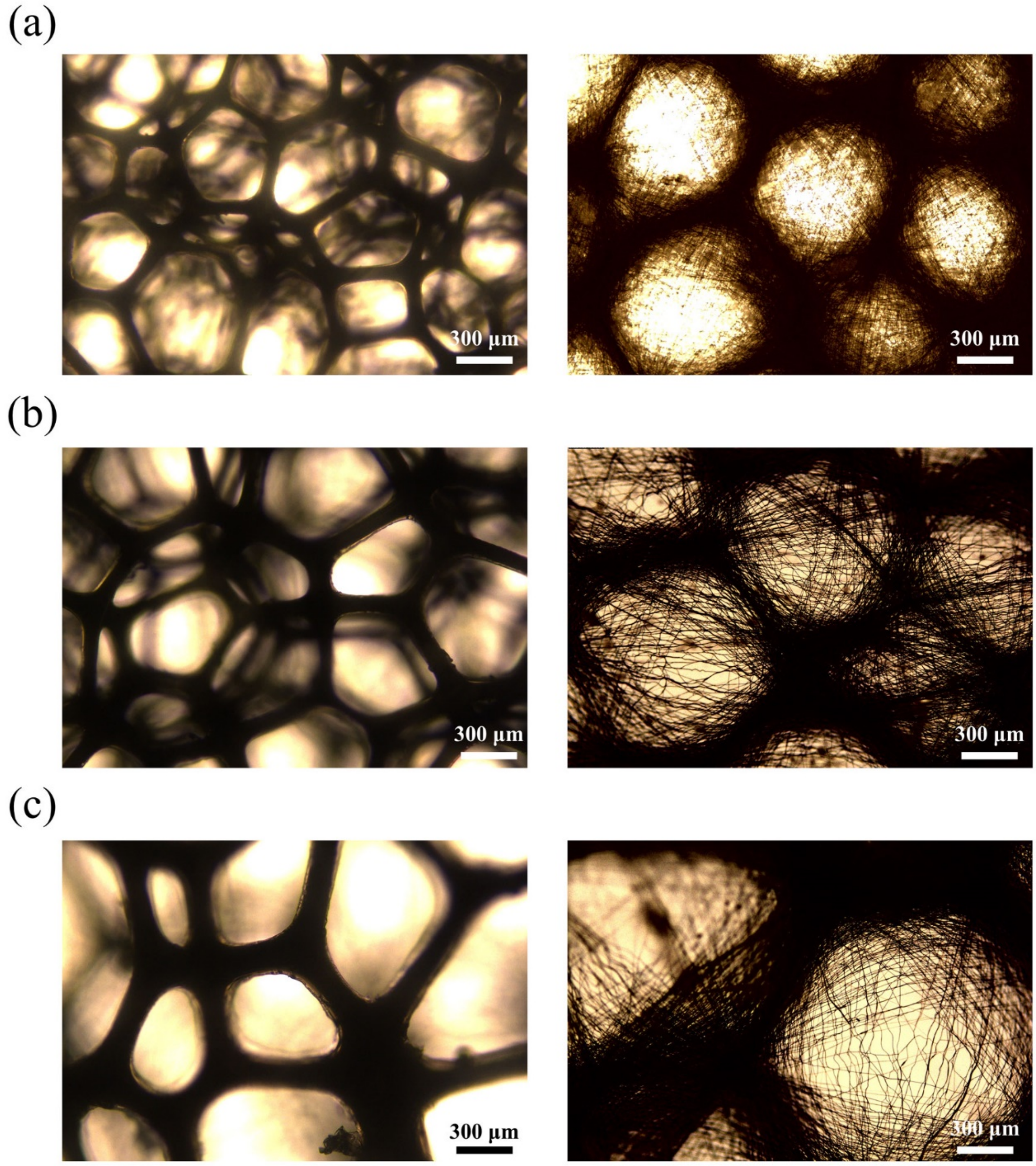

Fig. S3. (a) The optical photograph of 60 mesh foam and corresponding ordered microporous fibrous membrane; (b) The optical photograph of 40 mesh foam and corresponding ordered mesoporous fibrous membrane; (c) The optical photograph of 20 mesh foam and corresponding ordered macroporous fibrous membrane.

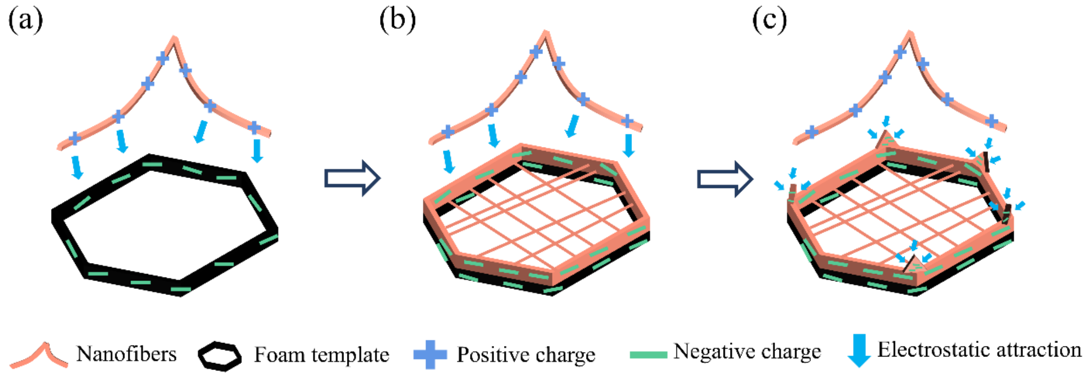

Fig. S4. (a) Schematic illustration of the positively charged nanofibers and the negatively charged foam template. (b) The growth process of two-dimensional honeycomb microstructure. (c) The growth process of two-dimensional honeycomb and three-dimensional spinous dual-coupled microstructures.

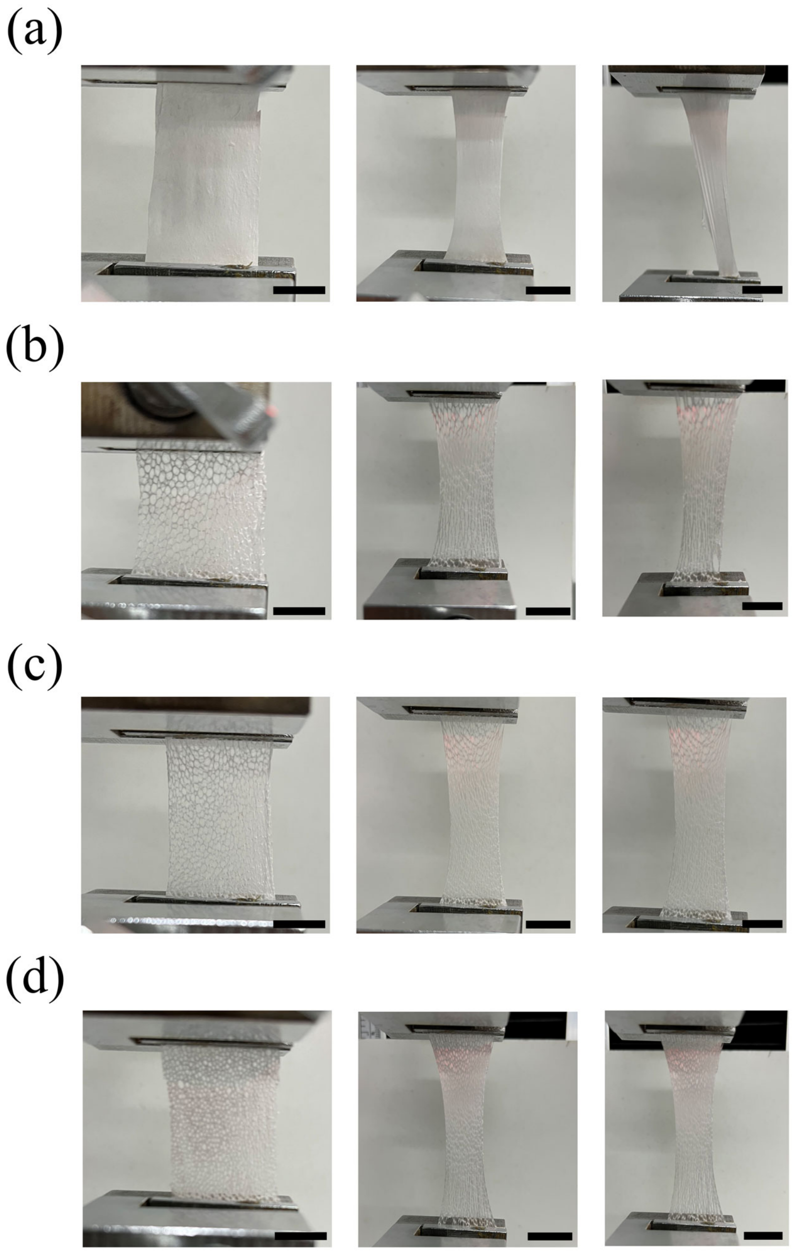

Fig. S5. The photographs of (a) the random porous fibrous membrane, (b) the ordered macroporous fibrous membrane, (c) the ordered mesoporous fibrous membrane and (d) the ordered microporous fibrous membrane at different stretching strains, respectively.

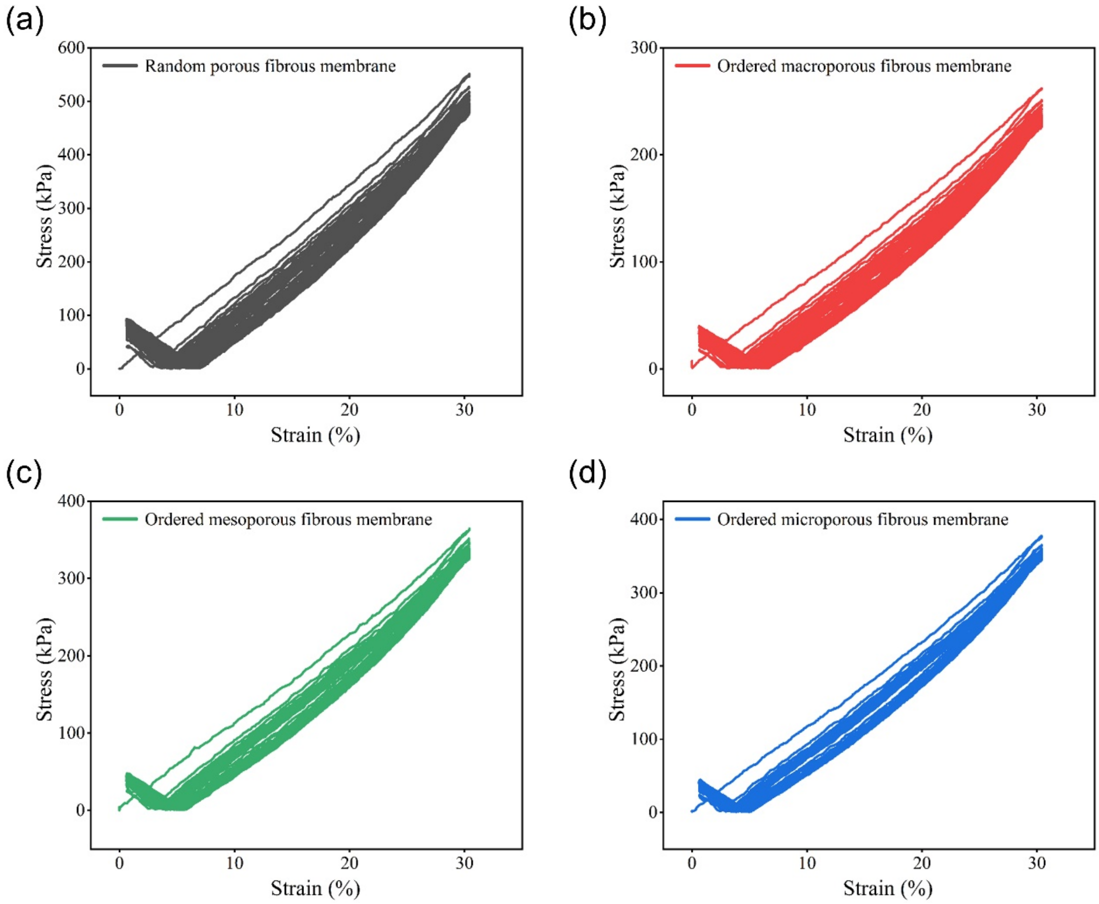

Fig. S6. The cyclic performance of (a) the random porous fibrous membrane, (b) the ordered macroporous fibrous membrane, (c) the ordered mesoporous fibrous membrane and (d) the ordered microporous fibrous membrane under the stretching status, respectively.

(a) (b)

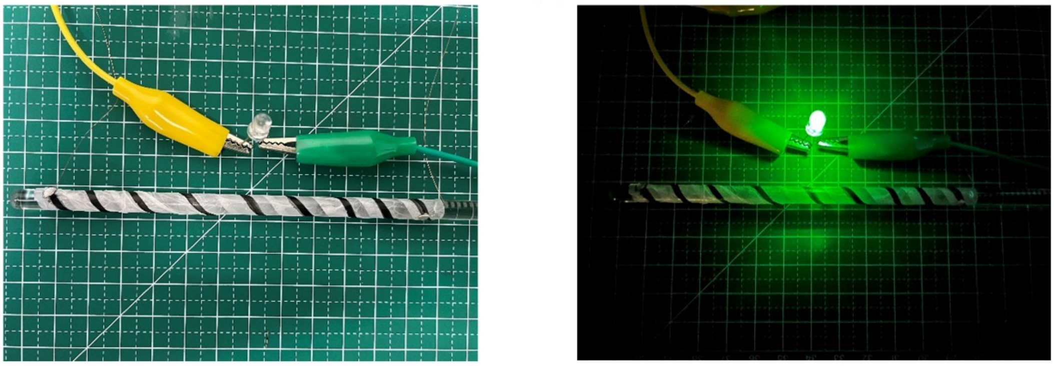

Fig. S7. Optical photographs of the CNT/ ordered microporous fibrous membrane acting as a conductor to light bulb.

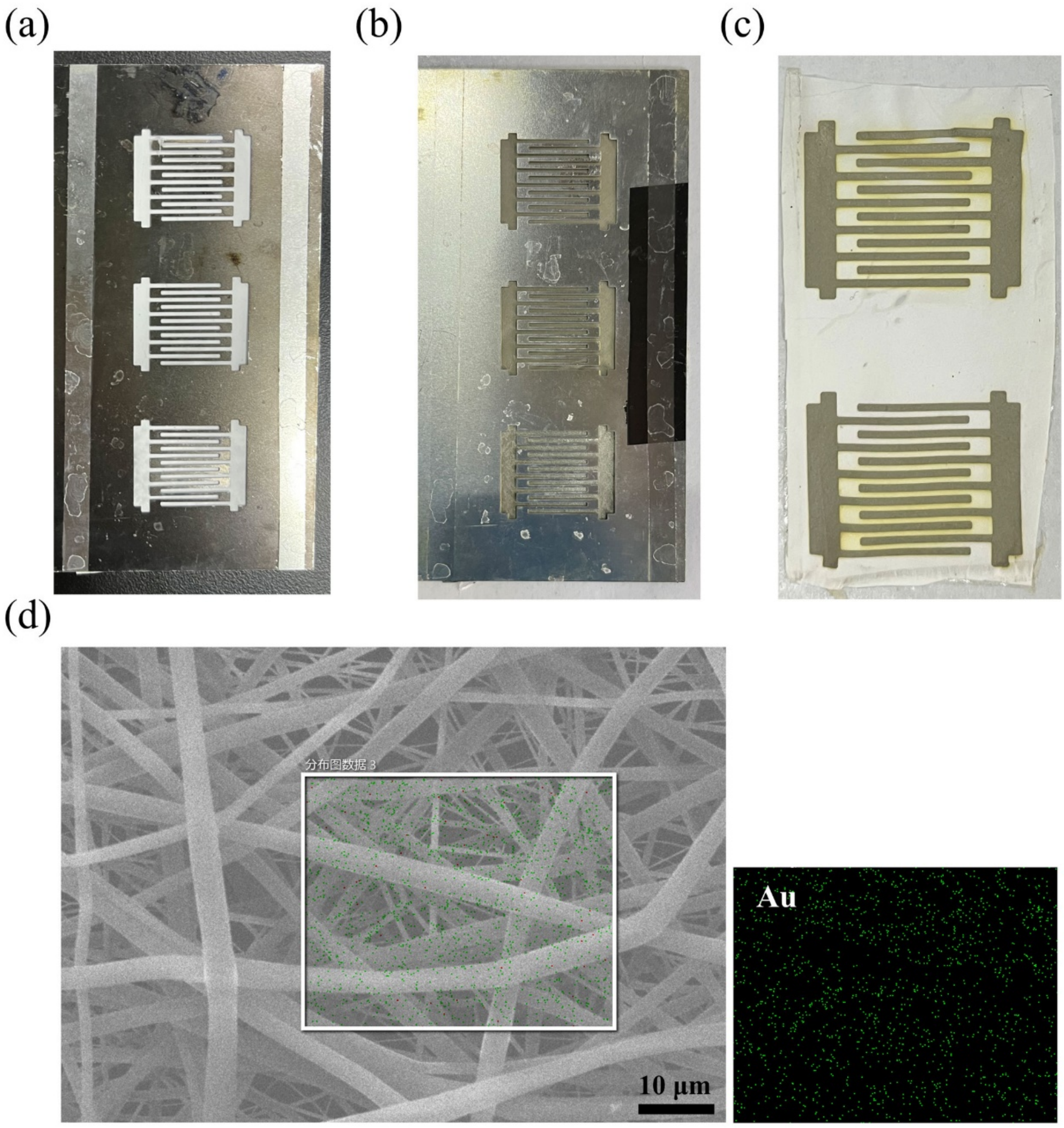

Fig. S8. (a) The optical photograph of a masking layer on the surface of fibrous membrane before magnetron sputtering. (b) The optical photograph of a masking layer on the surface of fibrous membrane after magnetron sputtering. (c) The optical photograph of breathable interdigital electrodes. (d) The Au elemental mapping image of the breathable interdigital electrode.

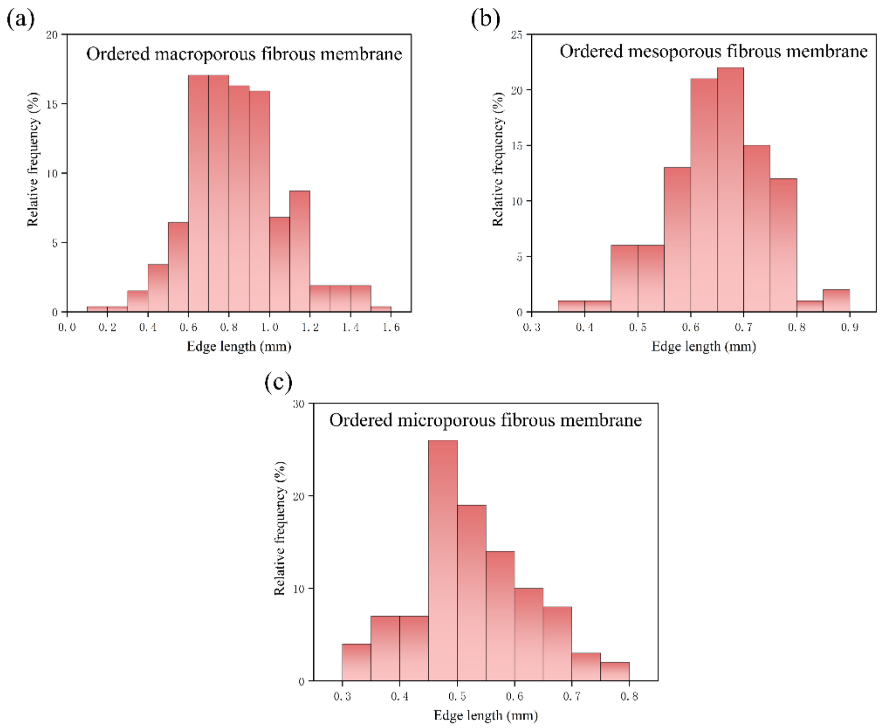

Fig. S9. The edge length distribution map of the (a) ordered macroporous nanofibrous membrane, (b) ordered mesoporous nanofibrous membrane and (c) ordered microporous nanofibrous membrane.

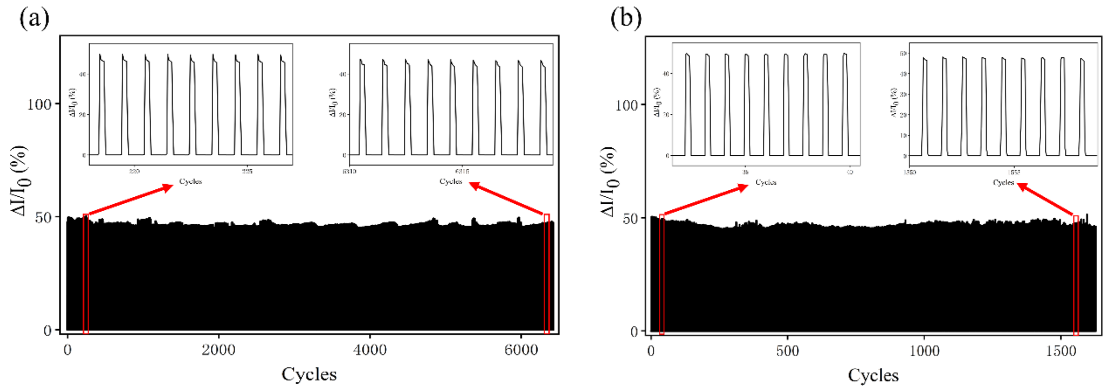

Fig. S10. (a) Cycling test curve of pressure sensor based on CNT/ordered microporous nanofibrous membrane at an ambient temperature of 60 °C. (b) Cycling test curve of pressure sensor based on CNT/ordered microporous nanofibrous membrane at an ambient humidity of 80%.

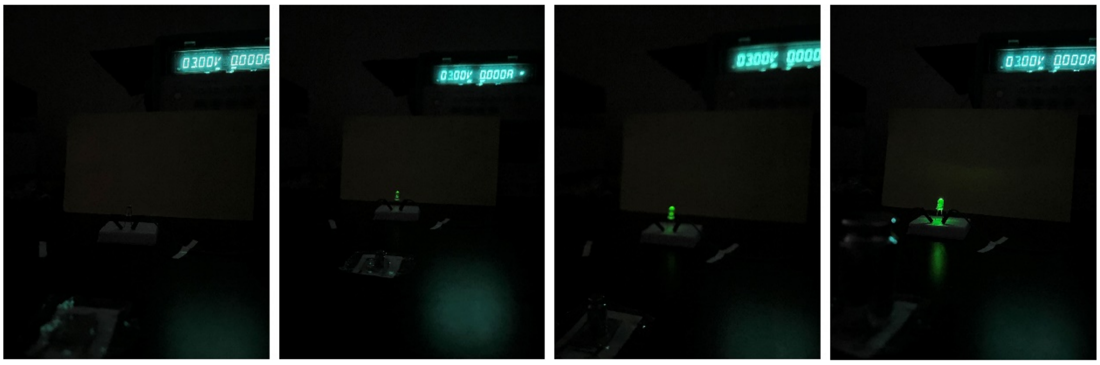

Fig. S11. Variation of the response of the LED luminance with the applied pressure on the dual-modality electronic skin.

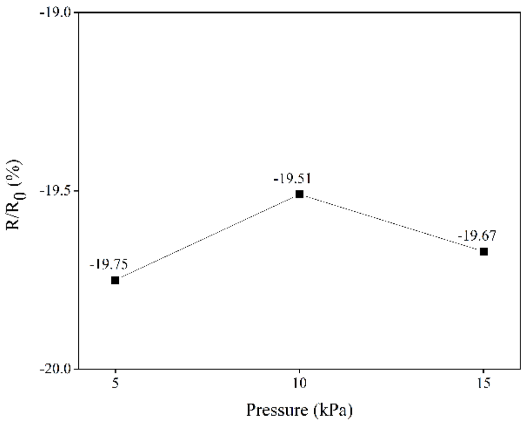

Fig. S12. The relative resistance change of the temperature sensing layer at different pressures (5, 10, 15 kPa) under constant temperature condition (50 °C).

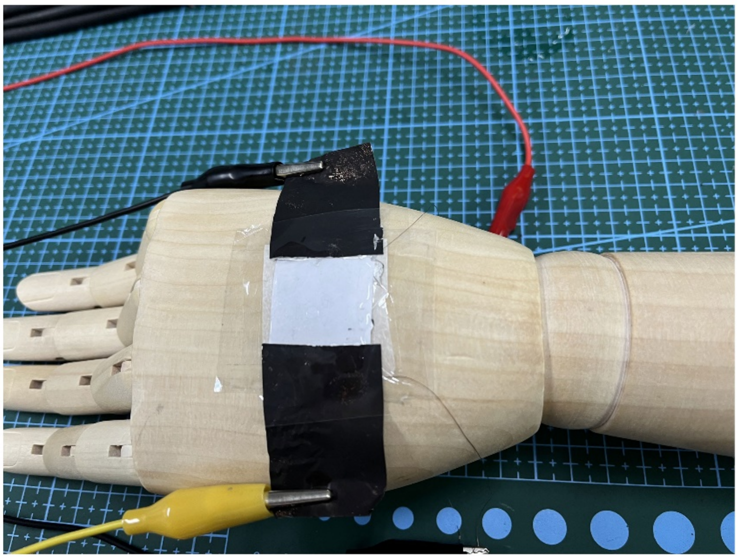

Fig. S13. Optical photograph of the dual-modality electronic skin.

Table. S1. Electrospinning process parameters for fabricating various nanofiber membranes.

Solvent	Solute (solution concentration)	Positive high voltage (kV)	Distance between needle and collector (mm)	Solution flow rate (mL/h)	Horizontal swing distance (cm)	Solution volume (mL)	Temperature (°C)	Relative humidity (%)
DMSO	TPU (25 wt%)	25	180	0.2	15	5	25±2	40±3

Table. S2. Comparison with traditional technologies.

Preparation method	Sample & structure	Advantages	limitations	Reference
Photoetching	Sensor imitating lotus leaf structure, combination of micropyramid and dual-helix structures, biomimetic nanopillar structure….	High precision (nanometer level), strong structural controllability	High cost, difficult to be prepared on a large scale	Nat. Mater. 2023[S1] Npj Flex Electron 2022[S2] ACS Nano 2023[S3]
3D Printing	Deep-trap hierarchical architecture, Multi-material composite structure, 3D lattice structure, tilted microhair arrays….	Customizable complex geometric structures, supporting multi-material integration	Limited accuracy (>10 μm), Limited material selection	Nano Energy 2023[S4] Appl Mater Today 2022[S5] Adv Sci 2024[S6] Adv Sci 2024[S7]
Chemical synthesis	Ionic crosslinked network hydrogels, Interpenetrating network hydrogels, Sliding ring network hydrogels….	High biocompatibility, self-healing properties	Insufficient long-term stability, Vulnerable to environmental influences	Nano Res 2024[S8] Nano Energy 2023[S9] Small 2025[S10]
Hydrothermal method	Layered cobalt sulfide@liquid metal, PVDF/CNF@ZnO composite membrane, ordered three-dimensional sheet microstructured aerogel…..	High specific surface area and porosity	Cumbersome post-processing steps	Nano Res. 2023[S11] Nano Energy 2024[S12] Chem Eng J 2024 [S13]
Template-assisted electrospinning method	Two-dimensional honeycomb and three-dimensional spiniform dual-coupled microstructure	High specific surface area, good air permeability	Poor structural uniformity	This work

Table. S3. The relationship between microstructural parameters and sensing performance metrics.

Structure	Honeycomb pore size (mm)	Edge length (mm)	Maximum sensitivity (kPa^{-1})	Sensing range (kPa)
Ordered microporous fibrous membrane	0.28	0.52	23	0-20
Ordered mesoporous fibrous membrane	0.46	0.65	14	0-20
Ordered macroporous fibrous membrane	0.62	0.83	11	0-20
Random porous fibrous membrane	None	None	5.3	0-8.6

[S1] Cheng W, Wang X, Xiong Z, et al., Frictionless multiphasic interface for near-ideal aero-elastic pressure sensing, Nature Materials, 2023, 22(11), 1352-1360
[S2] Li Y, Zhao M, Yan Y, et al., Multifunctional biomimetic tactile system via a stick-slip sensing strategy for human–machine interactions, NPJ Flexible electronics, 2022, 6(1), 46
[S3] Yao C, Sun T, Huang S, et al., Personalized machine learning-coupled nanopillar triboelectric pulse sensor for cuffless blood pressure continuous monitoring, ACS nano, 2023, 17(23), 24242-24258
[S4] Wang B, Gao M, Fu X, et al., 3D printing deep-trap hierarchical architecture-based non-contact sensor for multi-direction motion monitoring, Nano Energy, 2023, 107(2), 108135
[S5] Tao R, Shi J, Granier F, et al., Multi-material fused filament fabrication of flexible 3D piezoelectric nanocomposite lattices for pressure sensing and energy harvesting applications, Applied Materials Today, 2022, 29(12), 101596
[S6] Liu J, Zhang X, Liu J, et al., 3D printing of anisotropic piezoresistive pressure sensors for directional force perception, Advanced Science, 2024, 11(24), 2309607
[S7] Yu H, Guo H, Wang J, et al., Skin-Inspired Capacitive Flexible Tactile Sensor with an Asymmetric Structure for Detecting Directional Shear Forces, Advanced Science, 2024, 11(6), 2305883
[S8] Yang C, Ji C, Guo F, et al., An integrated portable bio-monitoring system based on tough hydrogels for comprehensive detection of physiological activities, Nano Research, 2024, 17(1), 321-332
[S9] Li J, Wang Z, Khan S A, et al., Self-powered information conversion based on thermogalvanic hydrogel with interpenetrating networks for nursing aphasic patients, Nano Energy, 2023, 113(10), 8612
[S10] Zeng Q, Qiao B, Xiao X and Li L, Self-Adhesive Gelatin/Slide-Ring Double-Network Hydrogel for Human Motion Sensing and Morse Code Communication, Small, 2025, 2(12) 2412665
[S11] Cao Y, Zhong H, Chen B, et al., Liquid metal-assisted hydrothermal preparation of cobalt disulfide on the polymer tape surface for flexible sensor, Nano Research, 2023, 16(5), 7575-7582
[S12] Zhu Q, Song X, Chen X, et al., A high performance nanocellulose-PVDF based piezoelectric nanogenerator based on the highly active CNF@ ZnO via electrospinning technology, Nano Energy, 2024, 127(10), 9741
[S13] Dong Z, Wang J, Li J, et al., Three-dimensional layered multifunctional carbon aerogel for energy storage and pressure sensors, Chemical Engineering Journal, 2024, 491(15), 1797